Journal of Materials Chemistry A

Accepted Manuscript

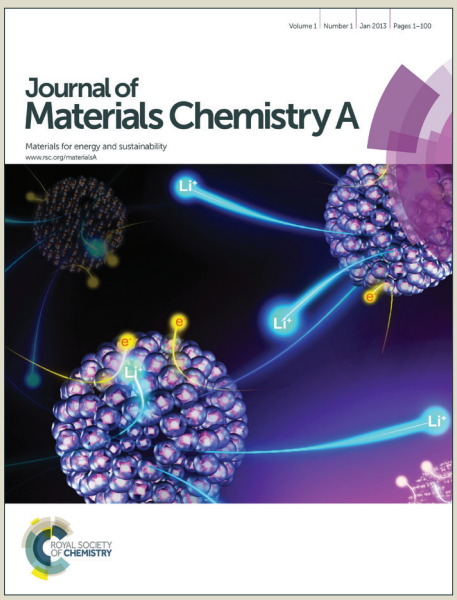

ROYAL SOCIETY OF CHEMISTRY

www.rsc.org/materialsA

Journal of

Materials Chemistry A

RSCPublishing

ARTICLE

Photogenerated electron reservoir in hetero-p-n CuO-ZnO nanocomposite device for visible-light-driven photocatalytic reduction of aqueous Cr(VI)†

Cite this: DOI: 10.1039/x0xx00000x

Jianyu Yu,‡ Shendong Zhuang,‡ Xiaoyong Xu,* Wenchang Zhu, Bing Feng, and Jingguo Hu*

Received 00th January 2012,
Accepted 00th January 2012

DOI: 10.1039/x0xx00000x

www.rsc.org/

Development of the visible-light-responsive catalysts with efficient recyclability has recently come into focus. Here, we report a three-dimensional (3D) heterohierarchical device consisted of two-dimensional (2D) p-type narrow bandgap semiconductor CuO nanosheets and one-dimensional n-type wide bandgap semiconductor ZnO nanorods, and fabricated via hydrothermal reaction after in-situ crystallization on Cu foil. Such a heterosturctured composite exhibited the significantly enhanced visible-light photocatalytic reduction capacity with stable recyclability to hexavalent chromium (Cr(VI)) compared with pure CuO nanosheets and ZnO nanorods. This improved photocatalysis was attributed to the synergistic actions of CuO and ZnO especially their formed p-n heterointerface for the extension of the solar absorption and the anti-recombination of photogenerated electron-hole pairs, evidencing the potential of p-n heterostructures for solar photocatalytic pollutant degradation or energy conversion. Moreover, the control of photogenerated electron reservoir cultivated on ZnO nanorods over the photocatalytic reduction activity was demonstrated, further clarifying the photocarrier dynamics and the photocatalytic mechanism in CuO-ZnO heterojunction. We hope the preparation of the 3D CuO-ZnO p-n junction device could provide a brand new approach to design versatile devices for solar energy conversion.

1. Introduction

Semiconductor photocatalysis has attracted widely attention due to the potential for hydrogen production and pollutant removal, which is a well-accepted strategy to simultaneously solve the energy and environmental crises, [1] since the photoelectrochemical water splitting over a titanium oxide (TiO_2) electrode had been first reported by Fujishima and Honda in 1972. [2] To date, various active wide-bandgap semiconductor photocatalysts have been rapidly developed as well, such as TiO_2, tin oxide (SnO_2) and zinc oxide (ZnO), *etc*. [3 - 6] Regrettably, wide-bandgap semiconductor catalysts could well operate under ultraviolet (UV) irradiation,[7] but they generally perform poorly under visible light. After all, UV light accounts for only a small fraction (4%) of the solar energy in comparison with visible light (43%). By contrast, the photoresponse of narrow-bandgap semiconductors extends much more into the visible wavelength range. Nevertheless, the narrow-bandgap semiconductors are difficult to maintain photoactivity over a long time due to fast recombination of photogenerated electron-hole pairs.[8] Therefore, any efforts to shift the optical response of a photocatalyst from UV to visible spectral range and to promote the photogenerated carrier separation would result in the positive effect on the photocatalytic efficiency.[9]

ZnO as an important n-type wide-bandgap semiconductor ($E_g \approx 3.37$ eV)[10] has been extensively researched in multiple fields, such as optoelectronic devices,[11] sensors[12] and photocatalysts,[13] because of its high fluorescence efficiency, carrier mobility and photocatalytic activity.[14,15] For the ZnO-based photocatalysts, to improve the visible-light-absorption and minimize the recombination of photogenerated electron-hole pairs, heterojunction constructing with narrow-bandgap semiconductors as a favorable design strategy has been widely explored.[16] As one of the most promising heterostructures, the p-n heterojunction enables the significantly enhanced capacities both of expanding visible-light absorption and retarding photogenerated electron-hole recombination.[17,18] Copper oxide

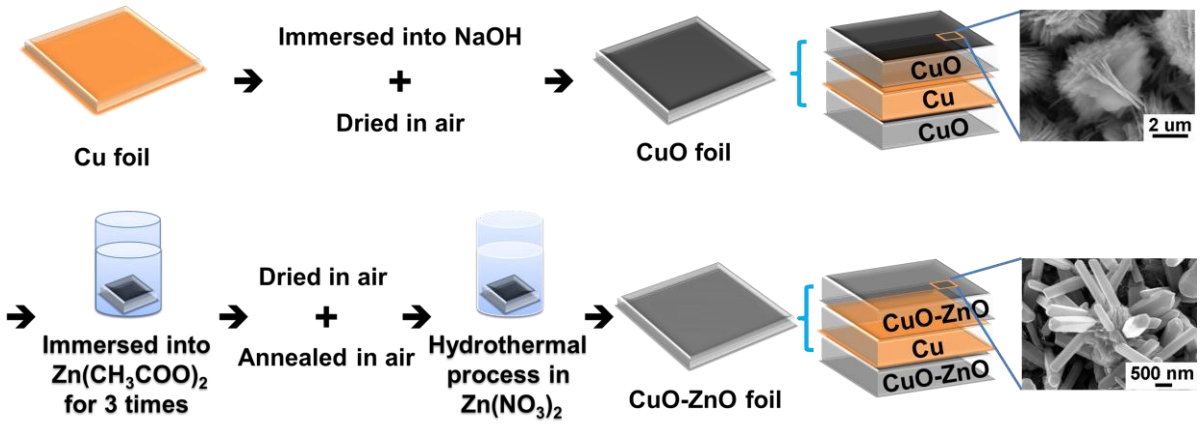

Figure 1. Scheme illustration for synthesis route of 3D CuO-ZnO p-n junction composite.

(CuO) as a p-type narrow-bandgap semiconductor ($E_g \approx 1.4$ eV) has a large absorption to visible light, although its photocatalytic activity is relatively low.[19] Moreover, based on the matched energy-band structure between CuO and ZnO, the reverse transporting of positive and negative charge carriers across the p-n heterointerface could be driven, which prevents the recombination of photogenerated electron-hole pairs and prolongs the carrier lifetime.[20,21] Therefore, the p-n CuO-ZnO heterojunction has been considered as a promising functional block for the generation and collection of electron or hole carriers in various photoelectrochemical (PEC) applications, such as gas detection, [22] self-cleaning,[20] and solar water splitting.[21] However, to the best of our knowledge, there are rare reports employing hetero-p-n CuO-ZnO composites for the photocatalytic reduction of hexavalent chromium (Cr(VI)), which is a typical heavy metal contaminant in the wastewater discharged from leather tanning, mining, electroplating and chromate manufacturing, etc. As one of the priority contaminants regulated in many countries, its removal is extremely urgent owing to its high toxicity and potential carcinogenicity.[23] The preferred treatment to Cr(VI) is to be reduced to the less harmful Cr(III), which could be precipitated in neutral or alkaline solutions as $Cr(OH)_3$.[24] In view of that the photogenerated electrons could be extracted and accumulated on the side of n-type ZnO, the CuO-ZnO p-n heterostructure could be supposed to activate the reduction of Cr(VI) under visible-light irradiation.

Herein, we synthesized first a large-area CuO microflower array formed by CuO nanosheets via in situ crystallization on Cu foil, then assembled a three-dimensional (3D) composite device consisted of two-dimensional (2D) CuO nanosheets and one-dimensional (1D) ZnO nanorods via hydrothermal growth of ZnO nanorods onto the CuO microflowers. Such a functional assembly performs a highly enhanced visible-light-driven photocatalytic reduction capacity with stable recyclability to Cr(VI) relative to pure CuO nanosheets and ZnO nanorods. Especially, the visible-light-activated electron reservoir is highlighted as the source for the photoreduction activity, focusing on the photocarrier transport in p-n junction and the photocatalytic mechanism of Cr(VI) reduction.

2. Experimental

2.1. Method summary

The 3D CuO-ZnO p-n junction composite was synthesized through hydrothermal assembly of ZnO nanorods onto CuO microflowers growing in situ on Cu foil, as illustrated in Figure 1. The formation of CuO-ZnO p-n junction was examined by X-ray diffraction (XRD), field emission scanning electron microscopy (FESEM) coupled with energy dispersive X-ray spectra (EDS) and high resolution transmission electron microscope (HRTEM) equiped with elemental mappings. The absorptive capacity to visible light and the photogenerated carrier transfer route in the CuO-ZnO nanocomposite were evaluated by the UV-vis absorption spectra, the photoluminescence (PL) spectra and visible-light-driven photocatalytic activity, combining with the coupled energy band structure based on the different work functions and the controlled experiments by adding respectively an additional electron provider rhodamine B (RhB, a photosensitizer) and an electron scavenger potassium persulfate ($K_2S_2O_8$).

2.2. Materials

Cu foils, hydrochloric acid (HCl, 36.0% - 38.0%), sodium hydroxide (NaOH, 96%), zinc acetate ($Zn(CH_3COO)_2{\cdot}2H_2O$, 99%), zinc nitrate ($Zn(NO_3)_2{\cdot}6H_2O$, 99%), hexamethylenetetramine ($C_6H_{12}N_4$), potassium dichromate ($K_2Cr_2O_7$, 99.8%), rhodamine B (RhB, 99.75%) and potassium persulfate ($K_2S_2O_8$, 99.5%) were purchased from Sinopharm Chemical Reagent Co., Ltd. (Shanghai, China). Deionized water was obtained from local sources. All materials were used as received without further purification.

2.3. Synthesis of CuO microflower array

The CuO microflower array was prepared via in situ engraving of the Cu foil (1 cm × 3.5 cm) based on previous report.[25] To

remove the surface impurities and oxide layers, Cu foil was first immersed in 3 M HCl aqueous solution for 10 min followed by rinsing with distilled water and absolute ethanol for three times, respectively. Subsequently, the cleaned Cu foil was immersed into a sealed beaker containing 10 mM NaOH aqueous solution at 60 °C for 21 h. After that, the foil was rinsed with distilled water and absolute ethanol for three times, and dried in air at 60 °C. The uniformly black surface layer of CuO microflower array growing on the Cu foil was obtained.

2.4. Preparation of 3D CuO-ZnO heterostructure composite

3D CuO-ZnO heterohierarchical configuration was obtained via a hydrothermal growth of ZnO nanorods on the CuO microflowers. First, the Cu foil with as-prepared CuO microflower array was immersed into the 0.005 M ethanol solution of $Zn(CH_3COO)_2$ for 15 s and then dried in air. After repeated for three times, it was annealed in air at 350 °C for 30 min, which would lead to the formation of ZnO seeds onto the surface of CuO nanosheets. Then, the CuO microflowers coated with ZnO seeds were put into Teflon-sealed autoclave containing 40 mL of an aqueous solution of equimolar (0.025 M) $Zn(NO_3)_2{\cdot}6H_2O$ and $C_6H_{12}N_4$, and maintained at 95 °C for 10 h. After the autoclave was cooled down naturally to room temperature, the as-synthesized sample was washed with distilled water and ethanol for three times, and dried in air at 60 °C. Finally, the CuO-ZnO heterojunction array on CuO foil was obtained. In addition, the pure ZnO nanorods were also prepared via the same route in the absence of CuO foil, after centrifugation with ethanol and deionized water for three times to fully remove the residual organic species and drying in air at 60 °C, as shown in Figure S1(Supporting Information, SI).

2.5. Characterization

XRD patterns were obtained by an X-ray diffractometer (Shimadzu XRD-7000) equipped with a Cu K_α radiation source, λ = 0.154 nm. The morphologies were observed using a FESEM (Hitachi S-4800 II) equipped with EDS and HRTEM (FEI Tecnai G2 F30 S-TWIN) coupled with element mapping. The diffuse reflectance absorption spectra (DRS) of the samples were recorded by a UV-vis spectrophotometer (Varian Cary 5000) in the range from 200 to 800 nm equipped with an integrated sphere attachment and with $BaSO_4$ as a reference. PL spectra were measured at room temperature with a luminescence spectrophotometer (Edinburgh EPL-375) using a Helium-Cadmium laser with a 325-nm excitation light.

2.6. Measurements of photocatalytic Activity

Photocatalytic activities of the catalysts were evaluated in term of photocatalytic reduction of Cr(VI) under visible light irradiation. Cr(VI) stock solution (20 mg/L) was prepared by dissolving $K_2Cr_2O_7$ into distilled water. After the catalyst was immersed into 40 mL of Cr(VI) solution, the resulted solution was magnetically stirred in the dark for 30 min at room temperature to establish adsorption-desorption equilibrium between the catalyst and the pollutant. Under stirring, the mixed suspension was exposed to visible light irradiation produced by a 300 W Xenon lamp with a 420 nm cut-off filter (λ > 420 nm, GHX-2 Photochemical Reactions Instrument, Yangzhou University City Science and Technology Co., Ltd.). The schematic of the photocatalytic reactor was shown in our previous report.[26] At at an interval of 20 min, 3 mL of the solution was extracted and monitored at the maximum absorption wavelength of Cr(VI) (352 nm), using a UV-Vis spectrophotometer (Shimadzu UV-2700). And the recyclability of the CuO-ZnO photocatalyst in this case was also studied after it was resinsed with ethanol and deionized water for three times. In addition, the controlled experiments by respectively adding photosensitizer RhB (1.6 mg) and electron scavenger $K_2S_2O_8$ (1.6 mg) during the photocatalytic reactions were performed to study their influences on photoreduction Cr(VI) activity of CuO-ZnO composite photocatalyst.

3. Results and discussion

3.1 Formation of 3D CuO-ZnO heterojunction composite

The crystal structure and phase purity of as-synthesized CuO and CuO-ZnO samples were characterized first by XRD patterns. As shown in Figure 2, the diffraction peaks of CuO crystallizing on Cu foil can be well indexed to CuO phase (JCPDS No. 44-0706), expect several diffraction peaks located at 43.1°, 50.2° and 73.9° coming from the Cu substrate, which indicates that the obtained CuO via the in situ engraving method is of high-purity crystallization without any other impurity phases like Cu_2O or $Cu(OH)_2$. After the hydrothermal growth of ZnO onto CuO-Cu foil, some additional diffraction peaks positioned at 31.5°, 34.2°, 36° and 47.2° emerge and can be assigned respectively to the (100), (002), (101) and (102) planes of wurtzite ZnO phase (JCPDS No. 36-1451), confirming the accession of ZnO crystals after the secondary growth.

The morphologies and microstructures of CuO and CuO-ZnO composite samples were characterized further by employing the FESEM, HRTEM, EDS and elemental mapping. Figure 3a and b show the FESEM images of CuO microflowers

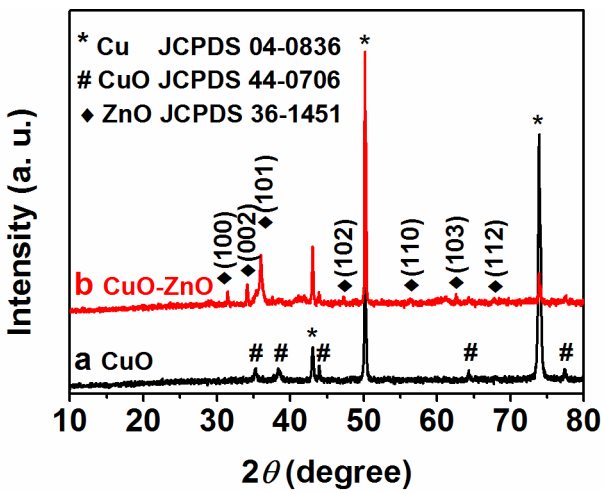

Figure 2. XRD patterns of (a) CuO and (b) CuO-ZnO composite.

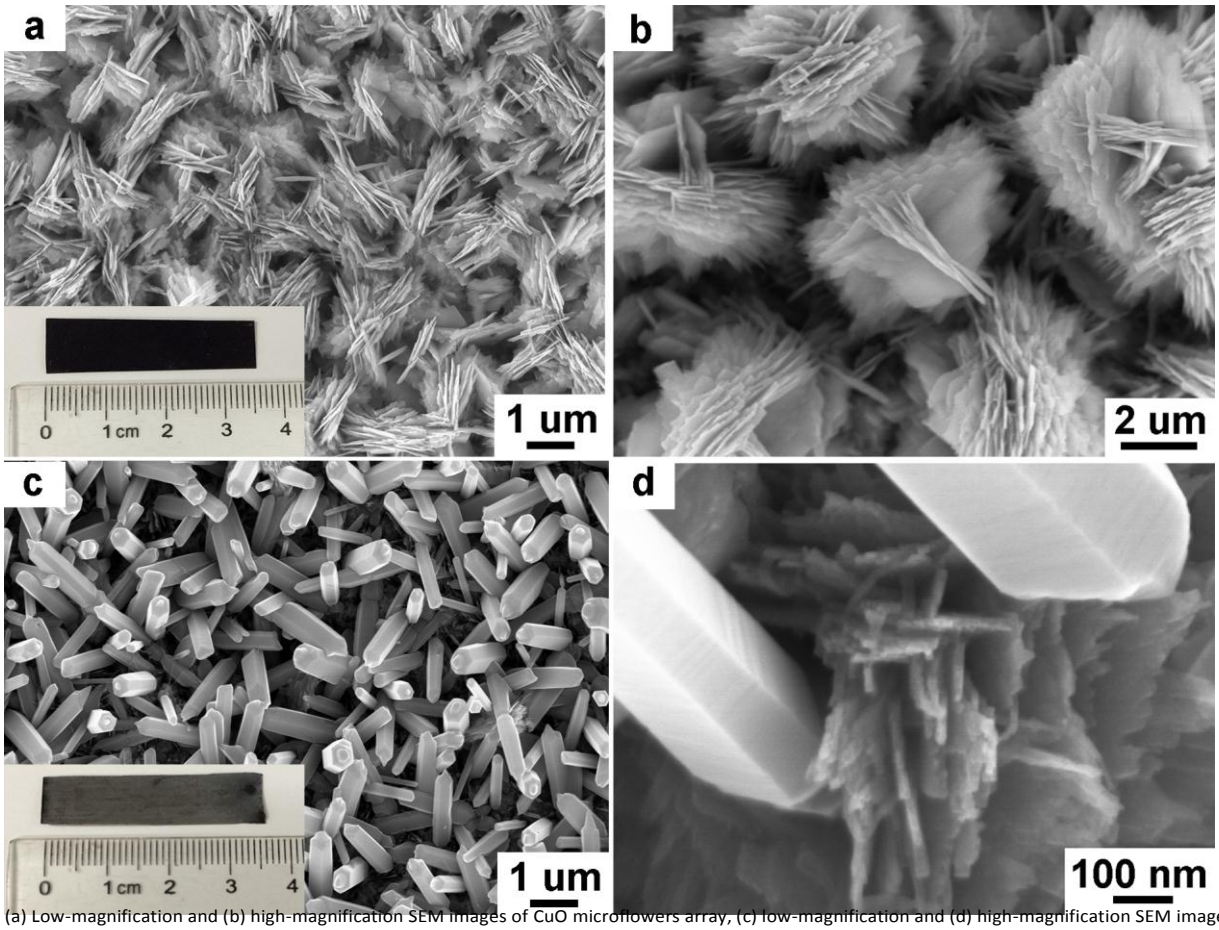

Figure 3. (a) Low-magnification and (b) high-magnification SEM images of CuO microflowers array, (c) low-magnification and (d) high-magnification SEM images of 3D CuO-ZnO heterojunction composite. Insets of (a) and (c) are the digital photos of CuO and CuO-ZnO foil, respectively.

grown on Cu foil with the different scale bars. Large-area CuO microflowers grow uniformly on Cu foil forming a favorable array structure, as shown in Figure 3a. The corresponding digital photo inserted into Figure 3a exhibits a homogeneous black surface, indicating the whole area of CuO coverage on the Cu subtrate. The amplified FESEM image in Figure 3b shows each CuO microflower is about 3 micrometer in diameter and composed of approximately standing nanosheets. After the hydrothermal growth of ZnO, the 3D CuO-ZnO hierarchical heterostructure was formed via the integration between ZnO nanorods and CuO microflowers, as shown in the FESEM images in Figure 3c and d. In the digital photo inserted in Figures 3c, the optical color of heterostructured sample becomes gray, which also suggests the successful secondary growth of white ZnO crystals.

Figure 4a shows the TEM image of an individual CuO-ZnO heteroblock exfoliated ultrasonically from the as-synthesized composite. One end of ZnO nanorod is wrapped by CuO nanosheets forming a hammer-like heterostructure, where the adamant connection between them was indicated with the effective binding against the strong ultrasound. A clear grain boundary can be found in the HRTEM image shown in Figure 4b. The interplanar spacings of 0.253 nm and 0.247 nm can be correspondingley indexed to CuO and ZnO crystalline phases, which directly confirm the formation of CuO-ZnO heterojunction.[27] The elemental mappings of Cu, Zn and O are shown in Figures 4c-e. The distribution of Cu element (Figure 4c) corresponds to the root segment, whereas that of Zn element (Figure 4d) fits well with the rod segment, presenting a clear constructional picture of heterohierarchical nanostructure. And the O element mapping (Figure 4e) is consistent with the TEM image of individual CuO-ZnO heteroblock, showing a uniform element distribution in the heteroblock. The corresponding EDS spectrum reveals the composition of Cu, Zn and O elements without any other impurity elements, as shown in Figure 4f. Therefore, the as-synthesized CuO-ZnO composite was clarified as a hierarchical heterostructure consisted of ZnO nanorods and CuO nanosheets with intimate heterointerfaces by the XRD, FESEM, HRTEM, EDS and element mapping analyses.

3.2. Absorption to visible light

To evaluate the capacity of absorpting visible light, the absorption spectra of as-synthesized ZnO nanorods, CuO foil and CuO-ZnO composite were recorded in Figure 5. The ZnO nanorods almost can not absorb any visible light due to its wide

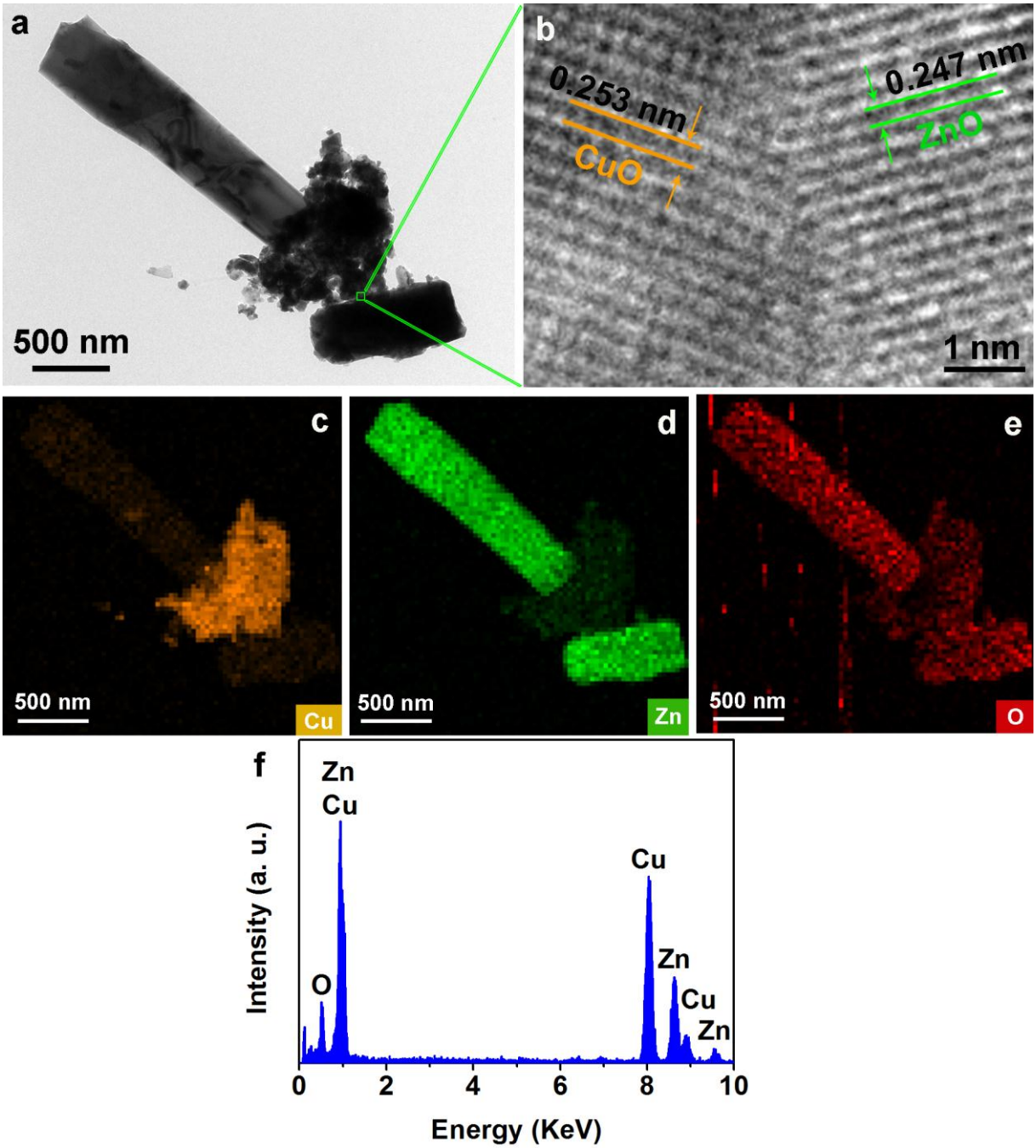

Figure 4. (a) TEM image, (b) HRTEM image, (c)-(e) Cu, Zn and O elemental mapping and (f) EDS of an individual CuO-ZnO heterojunction block.

band gap ($E_g \approx 3.14$ eV, Figure S2 (SI)), while the CuO-ZnO composite exhibits continuous absorption to the light in the range of 400-800 nm. This may be attributed to that the black CuO can well harvest visible light (as plotted in Figure 5) due to its narrow band gap ($E_g \approx 1.4$ eV)19 and provide the possibility of enhancing visible light absorption for the CuO-ZnO composite. Therefore, the combination of CuO and ZnO can effectively realize the optical response shifting of ZnO-based catalysts from UV to visible spectral range, which demonstrates the potential of the CuO-ZnO p-n junction heterostructure for visible-light-driven photocatalysis. This inference would be well confirmed by the photoreduction of Cr(VI) over the CuO-ZnO composite under visible-light irradiation as below.

3.3. Photocatalytic reduction of Cr(VI)

3.3.1. Photocatalytic activity

The photocatalytic activity of as-synthesized CuO-ZnO composite was investigated by monitoring the photoreduction

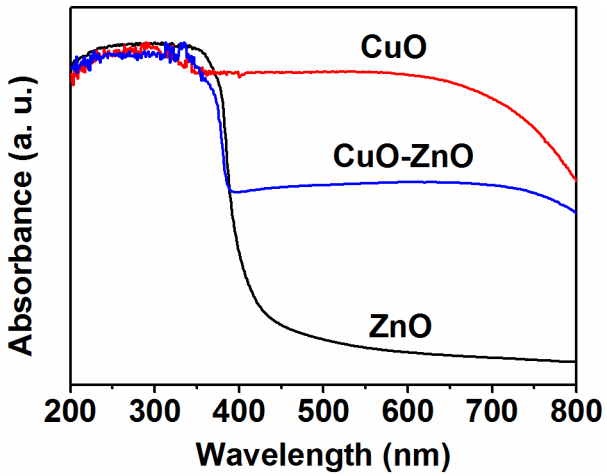

Figure 5. UV-vis absorption spectra of the as-synthesized ZnO nanorods, CuO foil and CuO-ZnO foil.

of Cr(VI). Figure 6a shows the time-dependent degradation curves of Cr(VI) without catalyst and in the presence of ZnO nanorods, CuO foil and CuO-ZnO composite foil under visible-light irradiation (λ > 420 nm) for 80 min. Herein, C_0 and C are respectively the initial concentration after the adsorption-desorption equilibrium and the actual concentration of Cr(VI) at different irradiation time, thus the lower C/C_0 denotes the higher photoreduction degree of Cr(VI). As shown in Figure 6a, Cr(VI) can hardly self-degradate under visible light (only about 0.5%), whereas in the presence of the CuO-ZnO composite, Cr(VI) can be almost completely degraded within 80 min and the photocatalytic efficiency is much higher than that of pure ZnO nanorods and CuO foil. The time-dependent evolution of absorption spectra and digital photos of Cr(VI) aqueous solution during the photocatalytic process with different catalysts are recorded Figure S3 and Supplementary Table 1. In additon, we found that the addition of RhB dye in Cr(VI) aqueous solution can further facilitate visible-light photocatalytic reduction of Cr(VI) over ZnO-CuO composite, moreover, RhB can also be simultaneously degraded, as shown in Figure S4 and Supplementary Table 1. Such a mutually promoted dual-degradation over p-n junction composite is of practical significance because organic dyes and heavy metals as two kinds of common pollutants usually coexist in the industrial wastewater.

3.3.2. Recyclability of CuO-ZnO composite

To evaluate the reusability of CuO-ZnO composite photocatalyst, we performed another three cycles of photocatalysis to Cr(VI) aqueous solutions in the presence of RhB, as shown in Figure 6b. No obvious change in photocatalytic efficiency indicates the macroscopical 3D CuO-ZnO composite foil as the conveniently separated photocatalyst can keep stable recyclability. Furthermore, the structural stability is also further confirmed by the XRD and SEM of CuO-ZnO sample after 4 cycles in Figure S5 (SI), where no noticeable changes are observed both in the XRD pattern and in the SEM morphology before and after the photocatalytic processes. These results illustrate that the present CuO-ZnO composite is stable, efficient and recyclable visible-light-driven photocatalyst for the Cr(VI) reduction.

3.3.3. Visible-light-driven photocatalytic mechanism of CuO-ZnO catalyst

Although the wide-bandgap ZnO has low absorption to visible light and poor visible-light photocatalytic capacity, the present CuO-ZnO composite performs excellent visible-light photocatalytic degradation,, which must be closely related with the contribution from CuO. First, CuO is a narrow-bandgap semiconductor, where the photogenerated charges can be activated by visible light, as supported by the absorption spectra

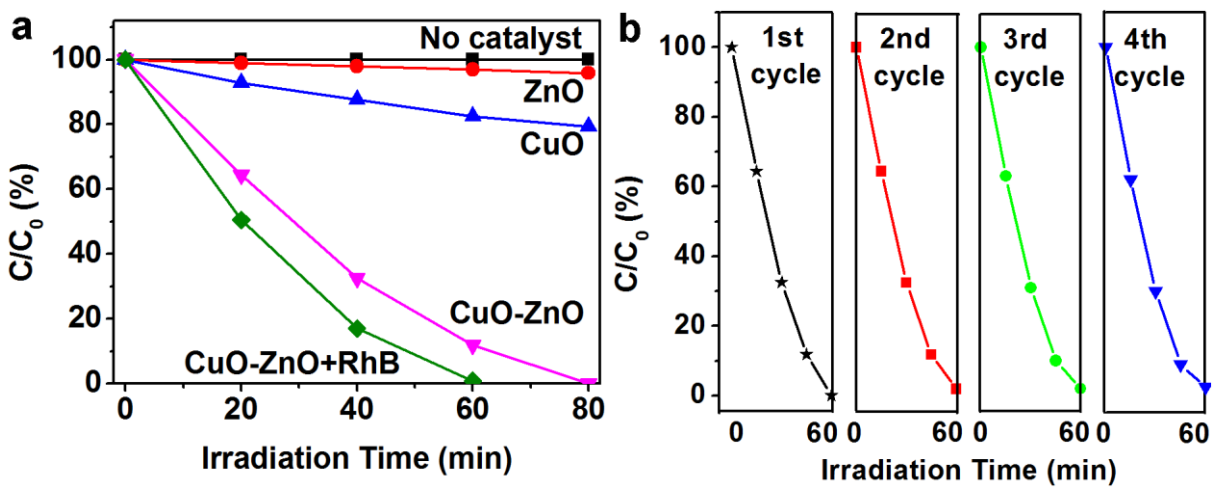

Figure 6. (a) Degradation curves of the Cr(VI) aqueous solutions containing different photocatalysts under visible light irradiation (λ > 420 nm): no catalyst, ZnO nanorods, CuO foil, CuO-ZnO composite foil and CuO-ZnO composite foil with the addition of RhB dye as photosensitizer. (b) Photocatalytic efficiency of the- CuO-ZnO composite to Cr(VI) reduction in the presence of RhB dye for separate 4 cycles.

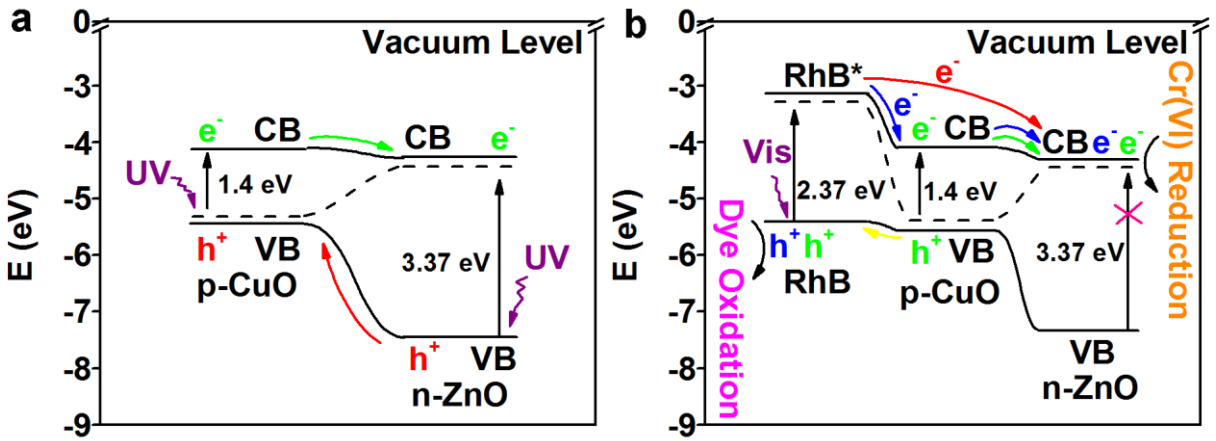

Figure 7. Schematic illustration of (a) migration path of photogenerated carriers in the CuO-ZnO p-n junction under UV irradiation (λ = 325 nm) and (b) photoreduction of Cr(VI) over the CuO-ZnO p-n junction catalyst in the presence of RhB under visible irradiation (λ > 420 nm).

in Figure 5. Second, the CuO-ZnO composite possesses stable p-n junction that can drive the photogenerated electrons and holes transport in reverse directions, and such an anti-recombination effect can be confirmed by the PL quenching of ZnO and CuO under the UV light (λ = 325 nm) (Figure S6) and time-resolved PL decay profile (Figure S7 and Supplementary Table 2). Based on the work functions of CuO (-4.07 eV) and ZnO (-4.35 eV) [21] as well as their band gaps (CuO, 1.4 eV; ZnO, 3.37 eV),[10,19] detailed theoretical band structures of CuO-ZnO p-n heterojunction in the state of pre-equilibrium, equilibrium in dark are shown in Figure S8. And the transfer path of photogenerated charge carriers as well as the theoretical band structures in the state of quasi-static equilibrium under UV irradiation (λ = 325 nm) and visible light (λ > 420 nm) are drawn in Figure 7a and b, respectively.[28-30] Under the UV irradiation (Figure 7a), the electrons photoexcited in conduction band (CB) of CuO transfer to the CB of ZnO and the holes photoexcited in valance band (VB) of ZnO transfer to the VB of CuO,[31] inducing the reverse transporting of electrons and holes at the CuO-ZnO interface. Under visible light (Figure 7b), although the electrons in ZnO cannot be excited from the VB to CB, but the electrons photoexcited in CB of CuO still migrate to CB of ZnO, propagating the so-called electron reservoir on the n-type ZnO side, which is supposed to be responsible for the enhanced photocatalytic activity of the CuO-ZnO heterostructure towards reduction of Cr(VI), as marked in green in Figure 7b. When adding RhB, because of the more positive work function of photoexcited RhB* (-3.08 eV)[26] than that of CuO (-4.07 eV) and ZnO (-4.35 eV)[21], RhB as the photosensitizer can also inject favorably additional photoinduced electrons into the CBs of CuO and ZnO to boost the electron reservoir through the formed downstream channel of electrons, as displayed respectively in blue and red in Figure 7b, thus photoreduction efficiency of Cr(VI) is further improved.

To confirm the role of visible-light-activated electron reservoir for the photoreduction of Cr(VI) over the CuO-ZnO composite, the effects of adding electron photosensitizer RhB and electron scavenger $K_2S_2O_8$ on the photocatalytic activities were comparatively analyzed. As shown in Figure 8, the introduction of RhB further increased the reduction efficiency of Cr(VI), while that of $K_2S_2O_8$ almost terminated the Cr(VI) reduction process.[32,33] The compared results evidently demonstrate that the electron reservoir photogenerated in the hetero-p-n CuO-ZnO composite indeed plays a motivational role to the photocatalytic reduction of Cr(VI), and the corresponding photocatalytic reactions may be expressed by the following equations (4)-(6). Noting that in the Cr(VI) aqueous solution with RhB, the CuO-ZnO composite catalyst not only reduces more efficiently Cr(VI) but also simultaneously degrades RhB, indicating the oxidation reaction of degrading RhB (equations (7) and (8)) can also activited by the accumulated holes from the photoexcited hole-like $RhB^{\bullet+}$ (RhB with a $hole^+$) (equations (1)-(3))[34] and from the VB of CuO, as shown in yellow in Figure 7b.

$$RhB\,(C_{28}H_{31}ClN_2O_3) + h\nu \rightarrow RhB^* \quad (1)$$

$$RhB^* \rightarrow e^- + RhB^{\bullet+} \quad (2)$$

$$RhB^{\bullet+} \rightarrow RhB + h^+ \quad (3)$$

$$CuO + h\nu \rightarrow CuO(h^+ + e^-) \quad (4)$$

$$CuO(h^+ + e^-) + ZnO \rightarrow CuO(h^+) + ZnO(e^-) \quad (5)$$

$$6e^- + Cr_2O_7^{2-} + 14H^+ \rightarrow 2Cr^{3+} + 7H_2O \quad (6)$$

$$h^+ + H_2O \rightarrow \bullet OH + H^+ \quad (7)$$

$$RhB + \bullet OH \rightarrow CO_2 + H_2O + NO_3^- + NH_4^+ + Cl^- \quad (8)$$

4. Conclusions

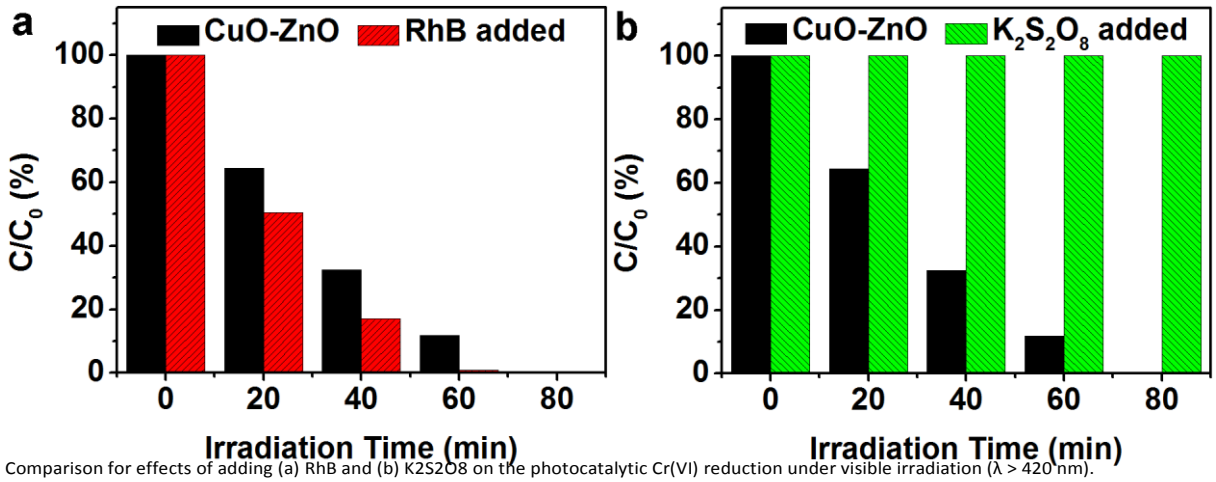

Figure 8. Comparison for effects of adding (a) RhB and (b) K2S2O8 on the photocatalytic Cr(VI) reduction under visible irradiation (λ > 420 nm).

In summary, the 3D flower-like CuO-ZnO composite device with intimate p-n heterointerface was synthesized via hydrothermal growth of 1D ZnO nanorods on the 2D CuO nanosheets. The as-synthesized CuO-ZnO heterostructure exhibits more superior visible-light-driven photoreduction capacity with efficient recyclability towards Cr(VI) relative to pure CuO nanosheets and ZnO nanorods, which is attributed that such a functional configuration can not only expand utilization of the visible light but also promotes the separation of photogenerated electron-hole pairs. Especially, the visible-light-activated electron reservoir developed during the p-n junction-driven charge migration process is revealed to be responsible for photocatalytic activity to Cr(VI) reduction by the controlled experiments of adding respectively electron photosensitizer RhB and electron scavenger $K_2S_2O_8$. Thus the CuO-ZnO heterostructured device is demonstrated as an effective visible-light-driven photocatalyst for environmental remediation or solar energy conversion.

Acknowledgements

This work was supported by the National Natural Science Foundation of China (Grant Nos. 11104240 and 11374253), the Jiangsu Government Scholarship for Oversea Studies in 2012 and the Innovation Projects (Grant Nos. 120801112 and 120804123) of Yangzhou University in 2014. And we thank the Testing Center of Yangzhou University for technical support.

Notes and references

School of Physics Science and Technology, Yangzhou University, Yangzhou 225002, PR China. E-mail: xxy@yzu.edu.cn (X. Y. Xu), jghu@yzu.edu.cn (J. G. Hu); Tel.: +86 0514 87970587; Fax: +86 0514 87975467

† Electronic Supplementary Information (ESI) available: [SEM image of the as-synthesized ZnO nanorods, Variation of versus the photon energy of ZnO nanorods, Absorption spectra and corresponding photos of Cr(VI) aqueous solutions catalyzed by different catalysts for 80 min, Absorption spectra of Cr(VI) aqueous solutions and absorption spectra and corresponding photos of Cr(VI) aqueous solutions catalyzed by CuO-ZnO foil with the presnece of RhB for different time under visible light irradiation, Absorbances (A) and percentage (P) of RhB and Cr(VI) in the RhB and Cr(VI) mixed solution at 554 nm and 352 nm at different irradiation time, XRD pattern and SEM image of the recycled CuO-ZnO foil, as well as PL spectra of pure ZnO nanorods, CuO foil and CuO-ZnO composite excited at 325 nm, Theoretical band structures of CuO-ZnO p-n heterojunction, and Time-resolved PL decay measurements.]. See DOI: 10.1039/b000000x/

‡ These authors contributed equally to this work.

1 J. Zhang, J. G. Yu, M. Jaroniec and J. R. Gong, *Nano Lett.*, 2012, **12**, 4584.
2 A. Fujishima and K. Honda, *Nature*, 1972, **238**, 37.
3 Nakata, K.; Fujishima, A. TiO2 photocatalysis: Design and applications. *J. Photochem. Photobiol. C* **2012**, *13*, 169-189.
4 Y. C. Zhang, L. Yao, G. Zhang, D. D. Dionysiou, J. Li and X. Du, *Appl. Catal. B: Environ.*, 2014, **144**, 730.
5 M. Q. Yang, N. Zhang and Y. J. Xu, *ACS Appl. Mater. Interfaces*, 2013, **5**, 1156.
6 K. Hu, K. C. D. Robson, P. G. Johansson, C. P. Berlinguette and G. J. Meyer, *J. Am. Chem. Soc.*, 2012, **134**, 8352.
7 C. Tian, Q. Zhang, A. Wu, M. Jiang, Z. Liang, B. Jiang and H. Fu, *Chem. Commun.*, 2012, **48**, 2858.
8 X. Zhang, Y. L. Chen, R. S. Liu and D. P. Tsai, *Rep. Prog. Phys.*, 2013, **76**, 046401.
9 G. Xie, K. Zhang, B. Guo, Q. Liu, L. Fang and J. R. Gong, *Adv. Mater.*, 2013, **25**, 3820.
10 X. Xu, C. Xu, J. Dai, J. Hu, F. Li and S. Zhang, *J. Phys. Chem. C*, 2012, **116**, 8813.
11 A. Sandhu, *Nat. Photon.*, 2007, **1**, 38.
12 S. Koizumi, K. Watanabe, M. Hasegawa and H. Kanda, *Science*, 2001, **292**, 1899.

13 M. Behrens, F. Studt, I. Kasatkin, S. Kühl, M. Hävecker, F. Abild-Pedersen, S. Zander, F. Girgsdies, P. Kurr, B. L. Kniep, M. Tovar, R. W. Fischer, J. K. Nørskov and R. Schlögl, *Science*, 2012, **336**, 893.
14 Z. W. Pan, Z. R. Dai and Z. L. Wang, *Science*, 2001, **291**, 1947.
15 M. H. Huang, Y. Wu, H. Feick, N. Tran, E. Weber and P. Yang, *Adv. Mater.*, 2001, **13**, 113.
16 Y. Wang, R. Shi, J. Lin and Y. Zhu, *Energ. Environ. Sci.*, 2011, **4**, 2922.
17 S. Ida, A. Takashiba, S. Koga, H. Hagiwara and T. Ishihara, *J. Am. Chem. Soc.*, 2014, **136**, 1872.
18 F. Meng, J. Li, S. K. Cushing, M. Zhi and N. Wu, *J. Am. Chem. Soc.*, 2013, **135**, 10286.
19 B. J. Hansen, N. Kouklin, G. Lu, I. K. Lin, J. Chen and X. Zhang, *J. Phys. Chem. C*, 2010, **114**, 2440.
20 Z. Guo, X. Chen, J. Li, J. H. Liu and X. J. Huang, *Langmuir*, 2011, **27**, 6193.
21 A. Kargar, Y. Jing, S. J. Kim, C. T. Riley, X. Pan and D. Wang, *ACS Nano*, 2013, **7**, 11112.
22 Q. Simon, D. Barreca, A. Gasparotto, C. Maccato, E. Tondello, C. Sada, E. Comini, G. Sberveglieri, M. Banerjee, K. Xu, A. Devi and R. A. Fischer, *ChemPhysChem*, 2012, **13**, 2342.
23 G. Gollavelli, C. C. Chang and Y. C. Ling, *ACS Sustain. Chem. Eng.*, 2013, **1**, 462.
24 S. Wei, Y. Chen, Y. Ma and Z. Shao, *J. Molecul. Catal. A*, 2010, **331**, 112.
25 S. Yuan, X. L. Huang, D. L. Ma, H. G. Wang, F. Z. Meng and X. B. Zhang, *Adv. Mater.*, 2014, **26**, 2273.
26 S. Zhuang, X. Xu, B. Feng, J. Hu, Y. Pang, G. Zhou, L. Tong and Y. Zhou, *ACS Appl. Mater. Interfaces*, 2013, **6**, 613.
27 Z. Bian, T. Tachikawa, P. Zhang, M. Fujitsuka and T. Majima, *Nat. Commun.*, 2014, **5**, 3038.
28 M. T. Mayer, C. Du and D. Wang, *J. Am. Chem. Soc.*, 2012, **134**, 12406.
29 N. Liang, J. Zai, M. Xu, Q. Zhu, X. Wei and X. Qian, *J. Mater. Chem. A*, 2014, **2**, 4208.
30 N. Liang, M. Wang, L. Jin, S. Huang, W. Chen, M. Xu, Q. He, J. Zai, N. Fang and X. Qian, *ACS Appl. Mater. Interfaces*, 2014, **6**, 11698.
31 S. Jung and K. Yong, *Chem. Commun.*, 2011, **47**, 2643.
32 M. Q. Yang, B. Weng and Y. J. Xu, *Langmuir*, 2013, **29**, 10549.
33 M. Q. Yang and Y. J. Xu, *J. Phys. Chem. C*, 2013, **117**, 21724.
34 P. V. Kamat, *Chem. Rev.*, 1993, **93**, 267.

Table of contents entry

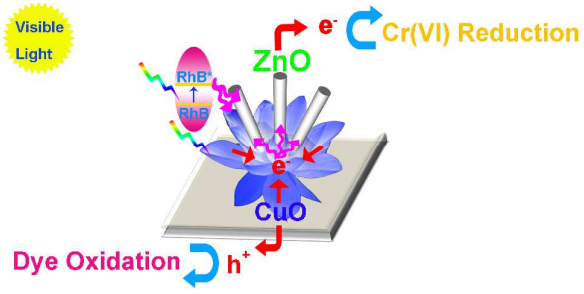

3D CuO-ZnO p-n junction hierarchical device was fabricated via sequential in-situ crystallization and hydrothermal reaction on Cu foil and exhibited enhanced visible-light photocatalytic reduction with stable recyclability to Cr(VI).